2023

Use of biomimicry model for the design of perforated composite plates

Modica-Cliff, G.

Modica-Cliff, G. (2023) 'Use of biomimicry model for the design of perforated composite platesl', The Plymouth Student Scientist, 16(1), pp. 49-85.
https://pearl.plymouth.ac.uk/handle/10026.1/21078

The Plymouth Student Scientist
University of Plymouth

Use of biomimicry model for the design of perforated composite plates

George Modica-Cliff

Project Advisor: Prof John Summerscales, School of Engineering, Computing, and Mathematics, University of Plymouth, Drake Circus, Plymouth, PL4 8AA.

Abstract

There are many practical reasons for making perforations in composites, which include reducing weight and for joining components. Nature often produces strong materials that have multiple perforations allowing organisms to survive in tough environments, biomimicry seeks to utilise these features for artificial solutions. The project proposes to investigate natural structures then using the information gained, to suggest methods by which we could design/make more efficient openings in composite structures. For example, to increase window size in aircraft structures without compromising strength or aerodynamics. Holes are usually made by machining however this project proposes a to use tree knots holes as a model to mould holes in composites. The project will validate its predictions through experimentation. Three types of sample plates were manufactured using resin infusion under flexible tooling (RIFT) and unidirectional fibres. Test samples using both a moulded and drilled hole are compared against each other and that of a control sample without a hole to investigate if tensile improvements have been made. Digital image correlation (DIC) analysis shows a difference in the failure mode of each. The project was limited due to time and resources, so could be usefully repeated with a larger test sample size and different hole sizes.

The results show that the moulded holes had a lower tensile strength but a higher tensile modulus than the drilled sample. The location of tow and stitching in the top layer did not appear to affect the results. However, the failure mode of the moulded samples was less catastrophic, showing a more gradual deterioration, which would prove advantageous in real-world scenarios, where products are monitored regularly. This process could be useful as it is reusable and saves on additional machining time and costs. Furthermore, there is no wasted material or risk of delamination and dust when installing components.

Keywords: biomimicry, perforated composite plates, unidirectional composite, open hole tensile strength, digital image Correlation.

Introduction

What is Biomimicry in the Context of Engineering?

Biomimicry is considered to be the area of science for developing technology inspired by nature, where forms, structures and mechanisms of organisms are the basic sources of influence for development of optimized design solutions (Boaretto et al., 2021). Evolution has allowed nature to provide solutions which are more complex and elegant than any artificial design, as organisms require optimum performance to survive (Bar-Cohen (Ed), 2006). Therefore, humans have frequently turned to nature for instruction and insight to help them to engineer solutions to their problems, leading to novel or improved devices (Vincent, 2016). Some famous examples are the flying machines developed by Otto Lilienthal in the 19th Century and to some extent Leonardo da Vinci 300 years earlier (Dickinson, 1999). It can clearly be seen that his studies of the anatomy of bats and birds, provided the basis for his gliding and flapping machines. Other examples include Gaudi's Sagrada Familia, figure 1, which includes many natural influences including buttressing and branching of its columns (Vincent, 2016). However, the application of natural inspiration is not always direct, elements from nature do not need to be applied to their intended use.

Figure 1: Sagrada Familia, biomimetic column (Kidd, 2019).

More recently designers have capitalised on a world of optimised design solutions in applications ranging from vaccine and enzyme development to robotics. Examples of the effective use of biomimicry include the use of artificial helicoidal architecture mimicking mantis shrimp exoskeletons to enhance impact toughness of wind turbine blades (Yin et al., 2020). The current era of sustainability has necessitated the development of low-impact ventilation systems. Both the East Gate Centre in Zimbabwe and, the CH2 building in Australia mimic the approach to temperature regulation and passive ventilation in the termite's mound (Abd et al., 2018). Adamu and Price (2015) have developed a feasible concept of a kidney inspired arrangement of natural ventilation with heat recovery systems suitable for retrofitting into existing buildings. Research has been carried out on replicating shark skin for its drag reduction and antifouling properties to be used on marine vessels (Pu et al., 2016).

Boaretto et al (2021) have highlighted the abundance of natural materials comprising of two or more materials with differing properties which cater for different demands. Some examples are insect cuticles, teeth, horns, ivory, seashells, wood and bones. Nature therefore provides a valuable lesson to improve the mechanical behaviour of synthetic fibre reinforced composites (Götz and Mattheck, 2001).

What are composites?

Composite materials are created by the consolidation of two or more materials to achieve properties that exceed those of its constituent parts (Barbero, 1999). Composite materials offer desirable properties including toughness, stiffness, and strength to relative weight, as well as corrosion resistance when compared to traditional engineering materials such as steel or aluminium (Grove, 2018). There are no off-the-shelf composite properties, as they are dictated by manufacturing quality, processes, and the lay-up itself (Åström, 2017). Furthermore, composites properties are highly dependent on orientation of the reinforcement and can therefore be tailored to suit design requirements (Clyne and Hull, 2019). Additionally, composites exhibit excellent fatigue resistance (Cripps, 2019) and durability in situations such as the marine environment. Consequently, composites are used to manufacture large structures such as aircraft fuselages and wind turbine blades (Sloan, 2012).

Composites presently constitute over 50% of the structural weight of some commercial airliners (Slayton and Spinardi, 2016). Although more costly to manufacture than aluminium components, composites compete by providing precision in the control of their properties and improved fuel efficiency by weight reduction (Warren, 2004).

Resin infusion under flexible tooling (RIFT) is a composite manufacturing method using a mould, consisting of a lower mould tool and a vacuum bag instead of an upper mould tool. Because a vacuum is used instead of external pressure, the mould tool can be made from low-cost materials (Barbero, 1999). RIFT is an economical manufacturing technique able to produce large structures where the employment of an autoclave is too expensive. Consequently, this method is favoured in aerospace, where the size of the autoclave restricts the size of the composite structures that can be manufactured (McGrane, 2001).

What are perforated composites?

The term perforated composite refers to intentional holes, slots or notches created during the manufacturing process, but not due to damage or failure. Perforated composite panels are widely used as structural members in weight dependent applications, because of their high strength-to-weight ratio. Further weight reductions can be achieved through the introduction of cut-outs or notches, this leads to greater fuel efficiency and performance (Lal et al., 2020). Perforations in composites are

predominantly required for mechanical joints, the hole allows fasteners to be used. Openings are also used for access panels, sound deadening systems, window frames and passage holes for utilities such as pipes and cables (Kumar et al., 2020). Furthermore, aircraft wings store fuel requiring openings to transport the fuel (Lin et al., 2020). The incorporation of bolts allows both assembly/disassembly, part replacement and ease of airworthiness certification (Galińska, 2020). Therefore, machined holes are extensively used in aerospace, with over 12,000 holes drilled into an Airbus A400M wing set (Sloan, 2012) and 8,000 in a Saab Griffin fighter (Åström, 2017). An extreme example of perforated composites are lattice structures used in aerospace (Vasiliev et al., 2012), which look similar to the skeletons of glass sponges.

How are Perforated Composites Made?

There are two ways of introducing holes into a composite component, during manufacturing or post-manufacture. Common machining techniques include drilling milling, and waterjet cutting. The advantage of machining is that it can be done at any time during the lifecycle of the product in a more flexible manner in terms of positioning. Additionally, it can allow for the realities of manufacturing, like tolerances, asymmetry and warping. However, there are disadvantages to machining as it can introduce defects including delamination, fibre and surface damage, which diminish the performance and reliability of the product (Worrall et al., 2020). Furthermore, introducing traditional joining methods like bolts and rivets, destroys the load-bearing fibres and introduces high local stresses (Burns et al., 2012). Moreover, due to their properties, composites wear down tools quickly leading to increased tooling costs (Yang et al., 2008) and introduce health concerns from dust and decomposition products. The disadvantages introduced by machining can be mitigated by incorporating the hole into the component design, however this introduces inflexibility and complexity to their manufacturing.

Holes in Nature

Holes and perforations have evolved to perform many varied functions in nature; holes can be used for joints, transportation of chemicals, as veins and digestive tissue and for reduction of weight such as in bones. These holes occur at all scales from nano to macro. Some exceptional examples of perforations in nature come from the shell structures of single-celled marine microorganisms. Radiolarians are microzooplankton, that vary in size from ca. 30–300 μm, that are known for their fragile skeleton of opaline silica (O'Dogherty et al., 2021) see figure 2.

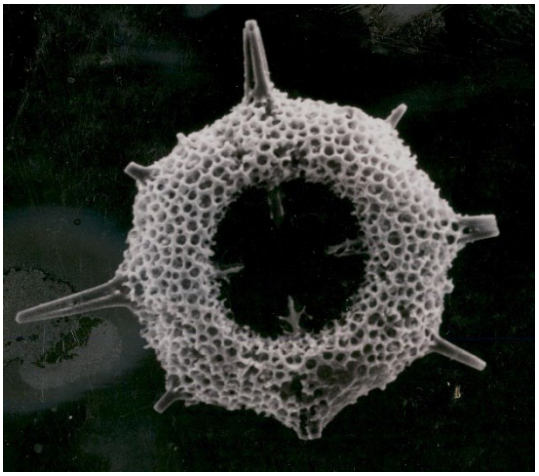

Figure 2: Radiolarian shell (Duran, 2015)

Another marine microorganism utilising similar shell structures are phytoplankton diatoms which are 20–200 μm in size (Round et al., 1990).Marine organisms like diatoms and radiolarians are very strong for their size and often have multiple orifices yet are tough enough to minimise predation, which makes them ideal models for translation into perforated composite products. Unfortunately, their small scale makes them impractical for this project. Consequently, other suitable natural models at a larger scale were researched and tree knots were selected as the most appropriate due to their strength (Polilov and Tatus, 2020).

Aims & Objectives

Aim

The project attempts to use biomimicry to improve the design of perforated composite products. This will be achieved by studying the features of an organism and applying these findings to develop an improved perforated composite plate.

Objectives:

1. Conduct a literature review to establish the state-of-the-art knowledge of the structural performance of natural holes or openings.
2. Choose an appropriate natural system from the literature survey.
3. Design a composite test component applying the knowledge specific features from the literature review findings.
4. Test the mechanical properties of the manufactured physical optimised model against an alternative and control.
5. Analyse results and write up final report.

Literature Review

A literature review was carried out following various avenues of research around the effect of perforations on material properties. Additionally alternative ways of reducing stress concentration were explored.

Stress Concentrations

Hu et al. (1997) studied the interlaminar shear stress in composites with holes. They were early adopters of finite element analysis (FEA). Traditionally, laminate plate theory assumes a planar stress, once holes are introduced this assumption no longer stands and a composite panel will exhibit interlaminar shear stress concentrations near the edges of the perforation. These may lead to the premature failure of the composite, due to matrix cracking from the free leading edge, which develop and can potentially rupture the laminate. They found an analytical model that agreed with their findings but did not use experimental results of their own, for validation. Cho and Rowland (2009) proposed that these interlaminar stresses could be managed by changing the orientation of local fibres around the hole. This study provided a process of modelling using FEA for the purpose of optimising orthotropic materials. However, their study was purely analytical and did not investigate mesh independency.

Influence of Multiple Holes

In the case of circular holes, Yeh and Le (1991) found that if the distances between holes is greater than 5 diameters of the hole itself the stress distribution approaches those of a single hole. Zhang et al. (2021) suggest that multi-site stress concentrations in the locality of holes interacted somewhat under both off and on axis loading, and stress distribution results around holes in multi-hole specimens were not significantly different to that of the single hole case. This indicates that a single-hole specimen can be used to

predict the behaviour of multi-hole specimens. However, the manufacturing methods or dimensions of test specimens were not given.

Hole Size

Mohamed Makki and Chokri (2017) investigated the effect of varying the diameter of a fixed width specimen on open hole tensile strengths. They used ASTM D-3039 as their standard for conducting tests and provided manufacturing details. They found that as hole size increased the strength and load bearing capacity of the plates decreased. Therefore, strength is inversely proportional to hole size in a fixed width specimen. Moreover, they identified the cause of this to be that the stress concentration at the hole increased with hole size.

Hole Shape

Low energy states are favoured by the forces of nature, causing the minimizing in the surface area of objects (Alderson, 2019). Therefore, circular holes are an effective natural method of forming openings as they have the lowest circumference to surface area, hence an efficient use of materials.

A notorious example of the importance of artificial hole shape in engineering was demonstrated by the de Havilland Comet. This aircraft was the first commercial jet airliner, entering service in 1952, but after a series of unexplained crashes the fleet was grounded in 1954. The inquiry into the crashes showed that the design had a severe weakness to fatigue crack growth in the aircraft skin around cut-outs such as windows and escape hatches caused by stress concentrations at the corners (Withey, 1997). This is supported by Watsar and Bharule (2015) who highlighted the significant stress concentration at the corners of triangular and rectangular holes. Their findings show that both rectangular and triangular holes have higher stress concentration factors than circular, while triangles have the highest stress concentrations factors for a given area. Their results from FEA were experimentally confirmed and manufacturing and material specifications were provided.

Reducing Stress Concentration

Tenchev et al. (1995) studied strengthening techniques for holes in composite laminates using ring reinforcement surrounding the hole and thus increasing the thickness. They also found that thickness of ring reinforcement increased with increasing hole diameter. They proposed this simple method of reducing stress concentration however they did not manufacture any plates. Guo (2007) expanded on this work by studying various reinforcements made from composite and metal. Their FEA and experiment found that the most effective reinforcement was the double ring in reducing stress concentration with the greatest reduction of local stress up to 53%. However, this technique adds weight, complexity to manufacturing and potential weak points at the adhesion joint.

This research indicates the widespread use of FEA with a combination of experimental validation. Another finding was the standardised open hole tensile test for composite panels, this gives a useful baseline for comparison of results.

Tree Knots

Knots in trees are the intersection between a branch and the trunk, and are therefore mechanically a very important aspect of trees, because they have to withstand a combination of static and dynamic loads, (Jungnikl et al., 2009) balancing strength, material usage and weight while maximizing energy absorption. Knots are the strongest part of the wood, as the branch is breakable, but it cannot be pulled out of the tree (Polilov and Tatus, 2020).

Ironically, knots in wood are traditionally viewed as defects, as they reduce strength in timber, affect the machining, drying and gluing properties of wood and have differential shrinkage and swelling rates when compared to that of the surrounding wood (Tsoumis, 1991). The adverse effect of knots is mainly due to local grain deviation. Evidence from Sofianto et al. (2019) shows that knots have a significant negative correlation with the predicted Young's modulus values due to the weakened neighbouring area of the knot compared to the surrounding wood. Furthermore, this work compared dead, living and empty knots, they found that dead knots and holes had less negative impact on the predicted Young's modulus than living knots. However, the results are purely theoretical predictions of one mechanical property, stiffness and no experimental validation was performed. This work does not compare the results to intentional holes like drilled holes, such analysis is unavailable. Furthermore, this analysis comes from the perspective of carpentry where the wood is processed, and holes are problematic.

Malakhov and Polilov (2016) used computational methods to model composite plates with fibres around a hole or any other geometric discontinuity, to calculate the stress concentration, fibre volume fraction and other mechanical properties. They were particularly interested in curvilinear fibre trajectories. Their conclusion was that by optimally reinforcing composites with curvilinear fibre alignment, there was a reduction of about 3-4 times in maximum stress and stress concentration of 3.8 times when compared to a unidirectional fibre arrangement. Additionally, there is a reduction in shear stresses, lowering the likelihood of failure around the holes.

Their computational results were validated against the experimental results of Mendoza Jasso et al. (2011) during the initial stages of modelling unidirectional composites. Their lay-up was made from fixed-angle unidirectional plies and a drilled hole rather than using fibre management to construct the hole. Once the results demonstrated a good match with the experimental data, they introduced curvilinear fibres into their FEA model. Unfortunately, this was not validated by experiment as none were available due to the complexities of manufacture.

Undoubtedly, practical limitations for this university project do not allow the production of such complex fibre management as shown in figure 3. Götz and Mattheck (2001) have compromised between feasible fibre lay-up whilst attempting biomimicry of a knot. They investigated the relationship between a fibre lay-up angle of +X°/0°/-X° patches on a base of biaxial fibre. They concluded that an optimum fibre lay-up angle of 13° gave the highest tensile strength whilst being feasible to manufacture. Their optimum angle result was found by computational methods and validated by experiment. However, their hole was drilled therefore fibre continuity was not maintained, in addition their patches were only unidirectional, so their transverse properties were severely compromised. Additionally, their results are not reproducible as they did not give manufacturing details such as method, materials, or dimensions of the specimens.

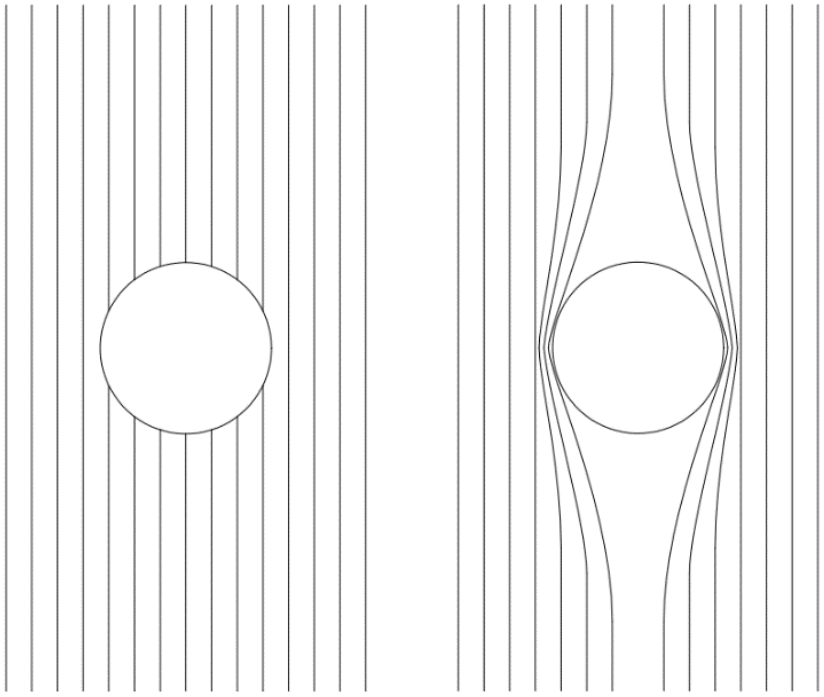

Figure 3: Comparison of fibre paths, left: fibres are discontinuous and cut by the hole like drilled holes, right: fibres are continuous.

The problems of knots associated with wood such as swelling and shrinkage due to grain density do not translate to composite materials. In fact, from the view of composite performance, aspects of knots can be implemented to great effect as shown by Malakhov and Polilov (2016) and Götz and Mattheck (2001). However, the literature review shows that only theoretical continuous fibres have been as the experimental holes are drilled.

Project Methodology

Biomimicry

Chosen Model

The tree knot hole identified in the literature survey will act as the model used to improve the stress concentration in holes in composites. To model this in composites, unidirectional (UD) fabric was used.

Drilled holes and biomimicry inspired holes will be compared against the performance of a plane control section with no hole. Figure 4 show tree knots which have inspired this.

Figure 4: Example tree knots showing curvilinear fibre path.

Constituent Materials

Fabric and Lay-up

Figure 5 shows the fabric used. It was Sigmatex MC8061276 UD carbon fibre which is 630 g/m^2, 400 tow/m manufactured in July 2003. It is held together by glass fibre stitching which maintains the alignment and produces a woven appearance, see figure 6. The true areal weight (Af) of 595 g/m^2 was found by the average of five 100 mm^2 samples. This reinforcement type was chosen as it most resembles the fibre within wood grain. During fabric preparation and sizing, all effort was made to minimise shearing and fraying of the reinforcement. The lay-up is three layers all at 0° ply angle [0°,0°,0°] with the top stitched face on the opposite of the mould tool face.

Resin System

Easy Composites IN2 epoxy infusion resin and AT30 fast hardener were used throughout. Additionally, the resin was mixed for 3 minutes before infusion and to the recommend 100:30 resin to hardener ratio from the datasheet (Easy Composites, n.d.).

Figure 5: Roll of UD carbon fibre fabric.

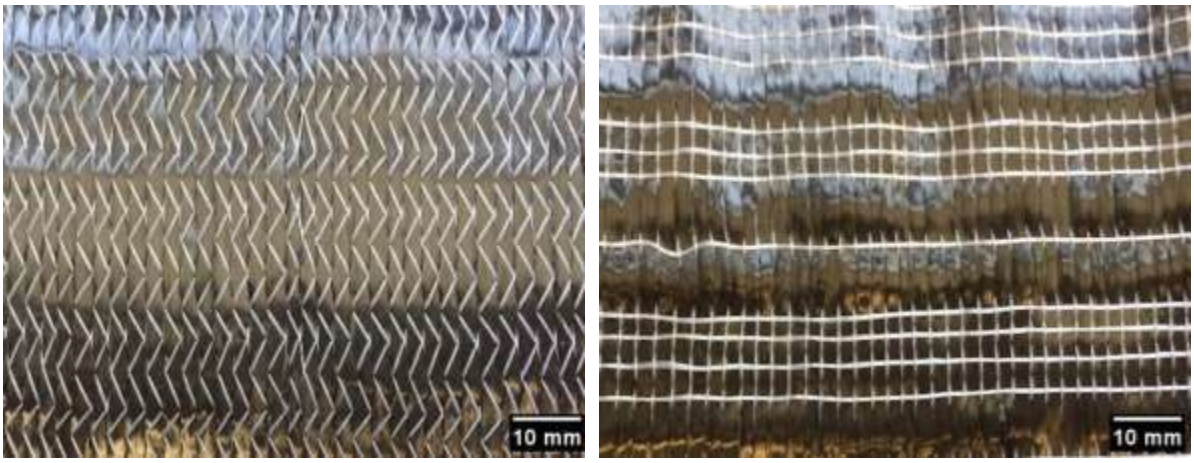

Figure 6: Detail of fabric, right herring bone stitch, left transverse stabilising threads.

Properties of Constituents

Table 1 shows the assumed property values. The resin properties used were the midpoint of the reported datasheet values. The fibre properties come from the carbon values suggested by Fu et al. (2000) as the manufacturer did not have a record of the raw material or exact construction.

Table 1: Modulus, strength and strain to failure of reinforcement and matrix.

Materials	Tensile Modulus (GPa)	Tensile Strength (MPa)	Strain at Failure (%)
Carbon Fibre	230	4900	2.1
IN2 Resin Matrix	2.8	71	8.0

Laminate Plate Manufacture

Resin Infusion under flexible tooling

Composite plates were manufactured using RIFT according to the method described in appendix 10.1. Figure 7 shows the set up. A risk assessment was carried out and is included in appendix 10.14. All plates were cured with the following schedule: 0.17°C/min ramp to 60°C, 6 h hold at temperature, then allowed to cool under natural conditions.

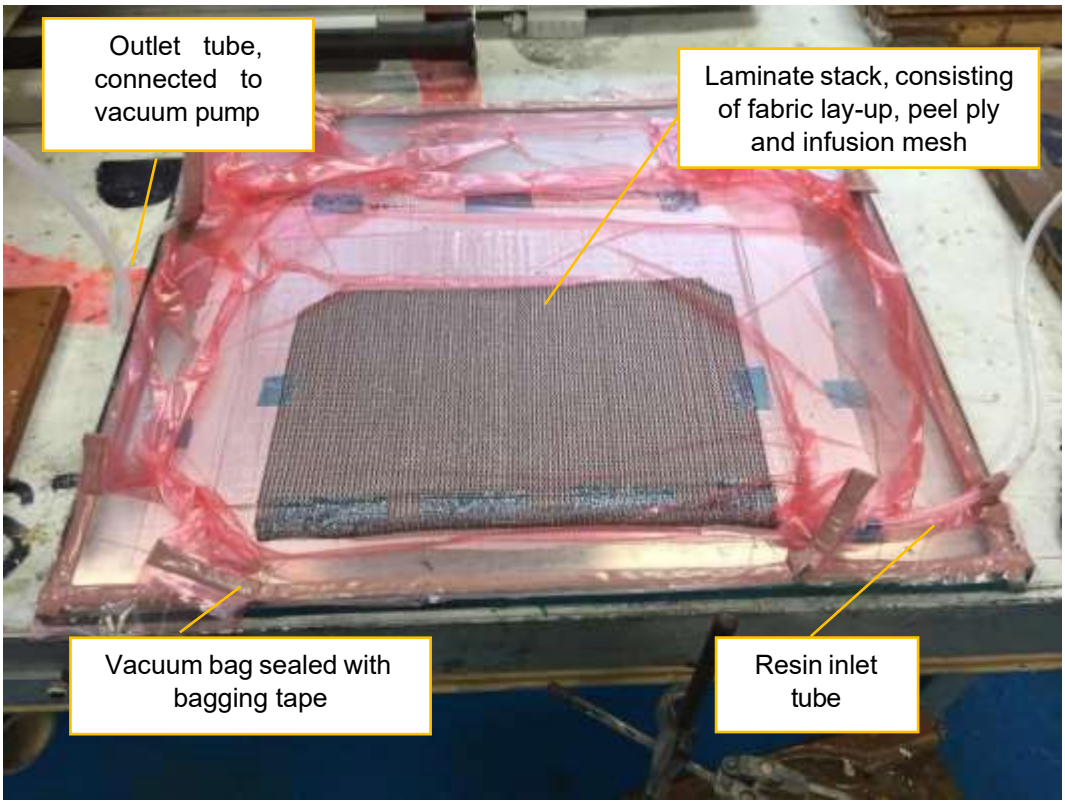

Figure 7: Annotated RIFT set up before infusion of resin.

Plate Types

Two types of plate were manufactured: drilled and moulded, full details can be seen in Table 2. The method of manufacture of the holes is the primary difference, except for the control specimens which have no holes. The specimens were cut from the large, cured plates using the Flow Mach 2 waterjet cutter in Brunel W006. Figure 8 shows the moulded plate post waterjet cutting.

Table 2: Plate dimensions and description.

Plate Name	Overall Plate Dimensions (mm)	Description	Specimen Dimensions (mm)
A	310 x 430	6 x control specimens 10 x drilled specimens	250 x 25
B	280 x 280	10 x moulded specimens	

Figure 8: Moulded plate once waterjet cut, note continuous profile leaving one uncut edge.

Moulded Holes

The method of moulding holes was inspired by knots in trees and was developed to be achievable with available time, equipment, materials and available technical staff. Figure 9 shows the MDF mould tool which produces a hole in the composite whilst maintaining fibre continuity. Figure 10 shows a detailed view of the pegs forming the holes. The pegs were made from PTFE and can be seen in figure 11, this material was chosen due to its non-stick (low surface energy) and thermal contraction properties which would allow easy removal once the composite had cured (TEKU, n.d). Figure 17 shows that despite these precautions, damage still arose in the demoulding process.

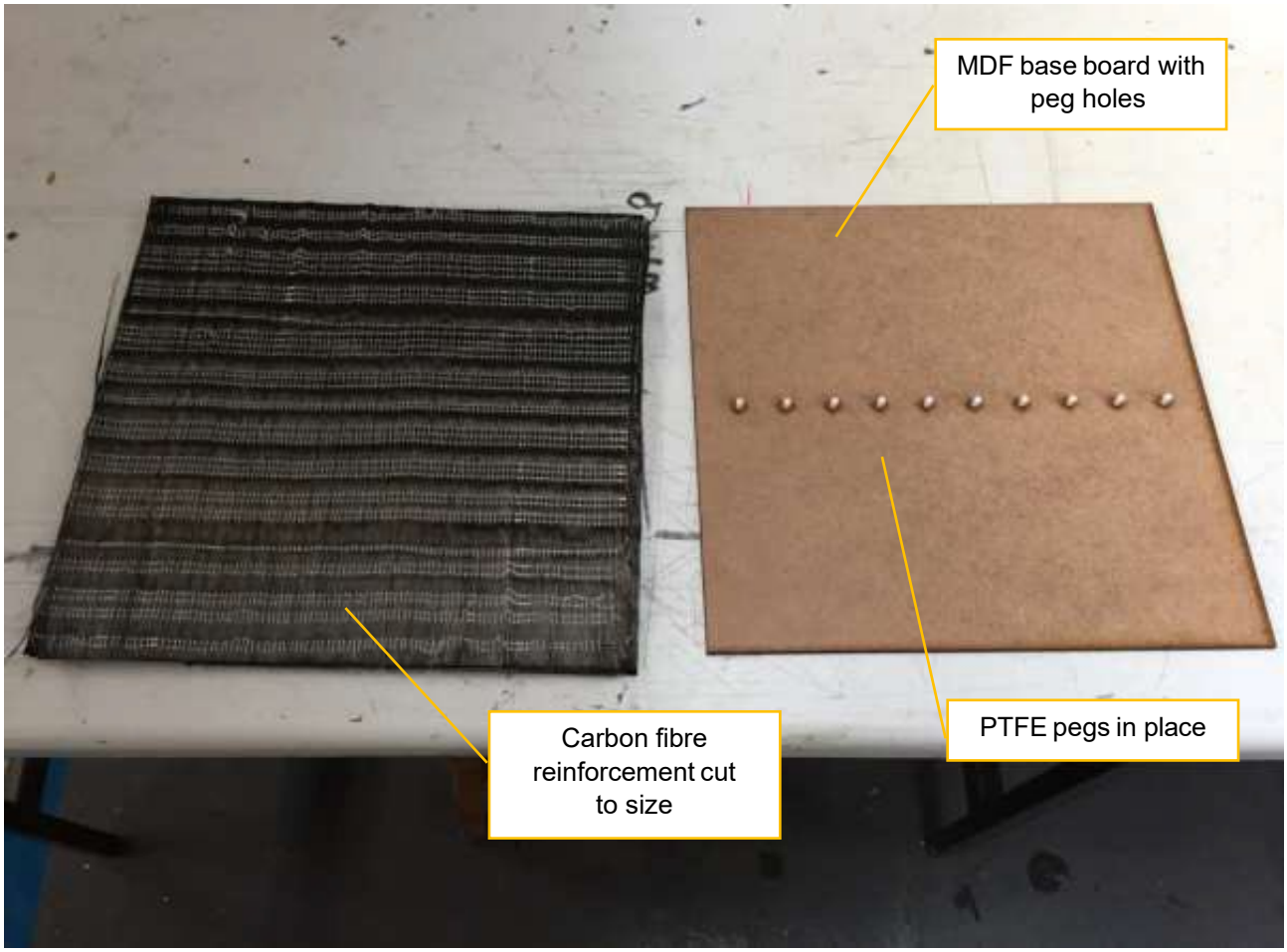

Figure 9: Annotated mould too next to cut up layup.

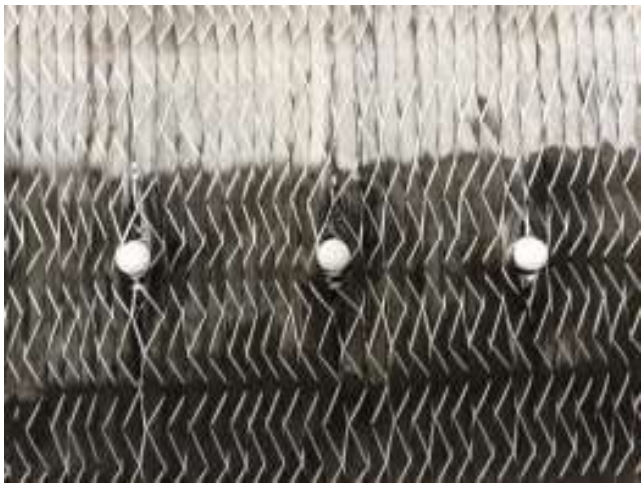

Figure 10: Detailed view of pegs through the fabric.

Figure 11: Peg next to a 20 pence coin to indicate scale.

Mechanical Testing

Tensile Test

The standard used was ASTM D5766 standard test method for open-hole tensile strength of polymer matrix composite laminates. The tensile test was performed with 2 mm/min tensile speed at room temperature of 26°C. Testing was conducted on an Instron 5582 with 100kN load cell which ran out of calibration on the 14 March 2017. The data was recorded as a load deflection curve. This was then adjusted to a stress-strain curve using the length and cross-sectional area (CSA) of each specimen. The gross CSA neglecting the hole was used as advised in the standard.

Table 3 shows the specimen geometry which is in accordance with the standard except the width/diameter ratio which should be 6. The hole size used was 4mm which gives a ratio of 6.25 as 4.16mm drill bits are uncommon. This is a suitable interpretation of the standard which states 6 (not 6.0). Control samples with no holes were tested along with specimens with circular holes either drilled using a tungsten carbide drill or moulded via developed method.

The specimens were prepared as in figure 12 as initial samples were slipping in the jaw grips, therefore invalidating the test, and damaging the samples.

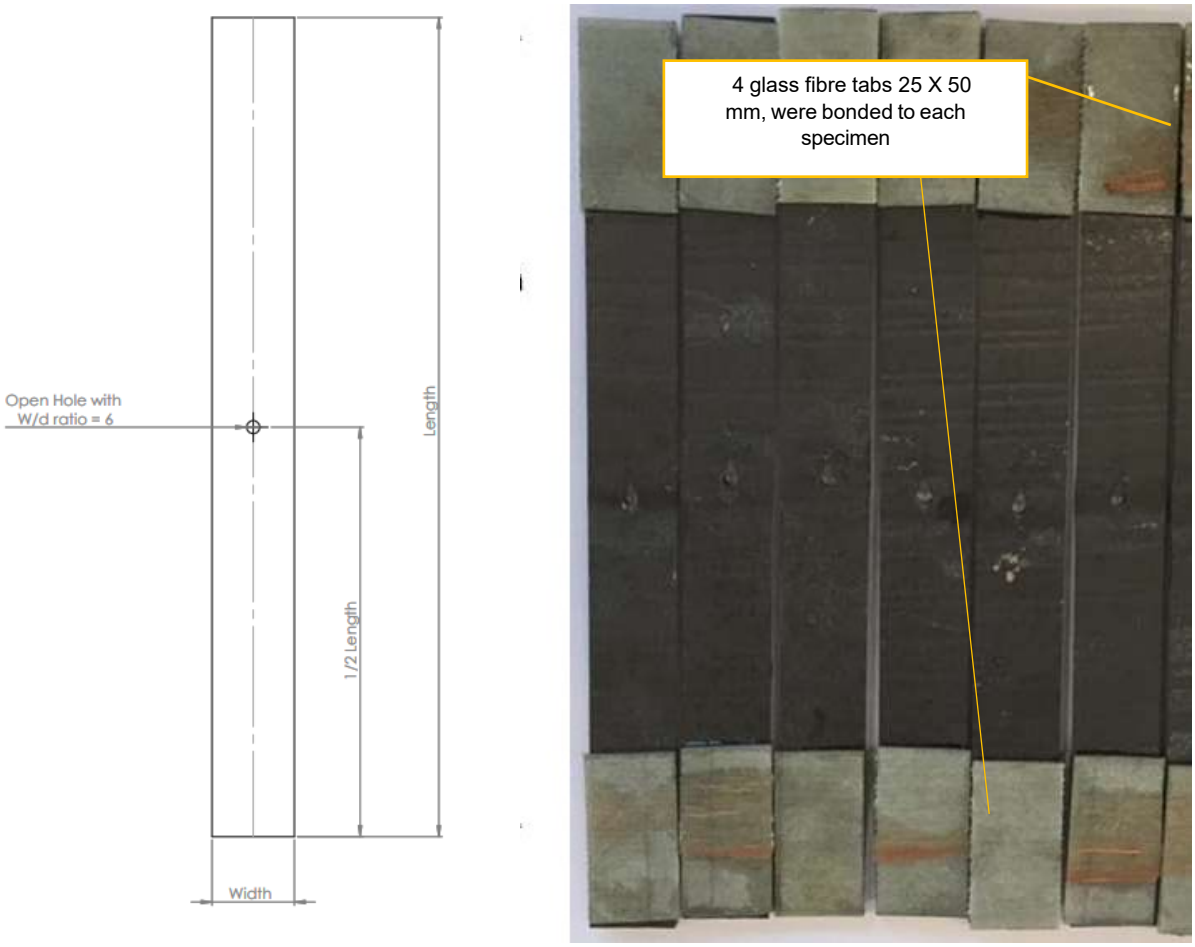

Figure 12: Left: schematic of open-hole tensile test specimen, right: annotated actual samples.

Table 3: Specimen geometry.

Specimen property	Unit	Value
Width W	mm	25
Length L	mm	250
Thickness t	mm	2
Hole diameter d	mm	4
Diameter to thickness ratio d/t	n/a	2
Width to diameter ratio W/d	n/a	6.25

Digital image correlation (DIC) was applied to some tests. DIC is a non-contact optical technique used to measure the displacement and deformation of an object by comparing images captured during loading. Samples are coated with a speckle pattern and the resolution is dependent on the quality of the coating. Figure 13 shows the coating applied during the sample preparation. The displacement of speckles in the images can be analysed to give the strain in the object which the software can convert into stress, figure 14 summarises the process.

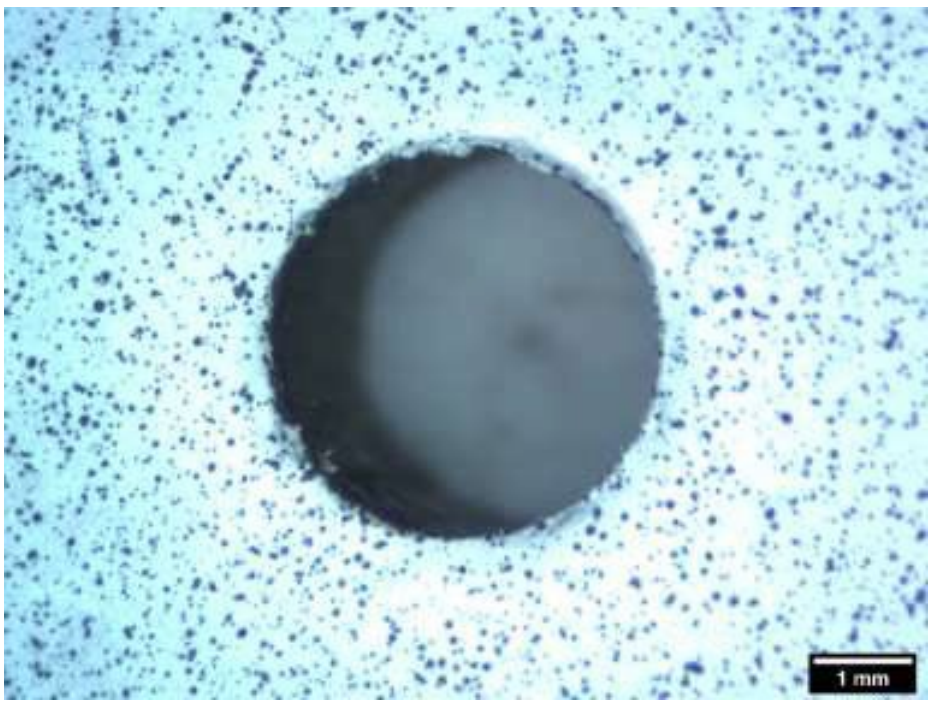

Figure 13: DIC speckle Pattern.

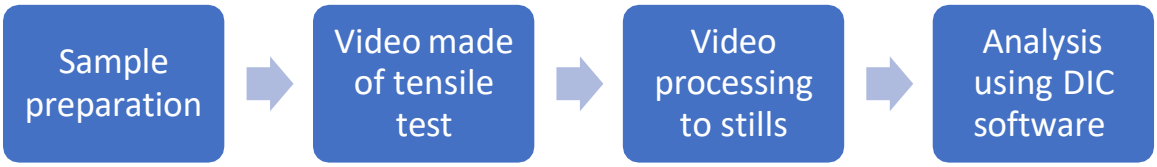

Figure 14: Flow chart of DIC process.

Fibre Volume Fraction

The fibre volume fraction (Vf) indicates the proportion of volume that fibre takes up out of the total composite expressed as a fraction. The Vf used in later composite property predictions was calculated using the following methods from Composite Research Advisory Group (CRAG) 1000 (RAE, 1988). CRAG 800 was required to calculate the density of the composite sample (ρc).

Composite Density Measurement

Both the density and resin burn off methods require the composite density value. Samples were taken from the plates, the mass of these were measured in air and then immersed and this apparent mass was recorded. Both values along with the density of water were input into Equation 1.

$$\rho_c = \frac{a\rho_w}{(a-b)}$$

$\rho_c = Composite\ Density\ (g/cm^3)$
$\rho_w = Water\ Density\ (g/cm^3)$
$a = Sample\ mass\ in\ air\ (g)$
$b = Sample\ mass\ in\ water\ (g)$

Equation 1: Test for measuring composite density.

Density Measurement Method

Draw a graph of density versus fibre percentage and input the composite density from above and read off the fibre volume fraction.

Laminate Thickness Method

Equation 2 shows the equation used to calculate the fibre volume fraction based on the average plate thickness of all samples.

$$V_f = \frac{A_F n}{\rho_f t}$$

$V_f = Fibre\ Volume\ Fraction\ (n/a)$
$A_F = Fabric\ Areal\ Weight\ (kg/m^2)$
$n = Number\ of\ Plies\ (n/a)$
$\rho_f = Fibre\ Density\ (kg/m^3)$
$t = Laminate\ Thickness\ (m)$

Equation 2: Fibre volume fraction, thickness method (RAE, 1988).

Resin Burn Off Method

This method involves weighing samples from each plate, and then placing them into the furnace at 550°C. The samples were measured until the weight stabilised, additionally control fibres were also measured for a correction of any fibre sizing being lost. These results are input into Equation 3.

$$V_f = \frac{100(M_f \rho_c)}{M\ \rho_f}$$

$V_f = Fibre\ volume\ fraction\ (\%)$
$M_x = Mass\ (g)$
$\rho_x = Density\ (g/cm^3)$
$f, c = fibre\ and\ composite\ respectivly$

Equation 3: Fibre volume fraction, burn off method (RAE, 1988).

Property Predictions

To validate various mechanical properties of the composite the following analytical methods were used.

Tensile Modulus

Rule of mixtures

Equation 4 shows rule of mixtures (RoM) equation which calculates the theoretical tensile modulus of the composite. The following assumptions lead to the simplification of the equation. The fibre orientation distribution factor can be set to one as the fibres are unidirectional. The fibre area correction factor, fibre diameter distribution factor and fibre length distribution factor can be set to unity. Assuming no void content.

$$E_c = \kappa \eta_d \eta_l \eta_o E_f V_f + E_m V_m$$

$$E_c = E_f V_f + E_m V_m$$

Where:
E_x=*Elastic modulus (Pa)*
V_x=*Volume fraction*
κ=*fibre area correction factor*
η_d=*Fibre diameter distribution factor*
η_l=*Fibre length distribution factor*
η_o=*Fibre orientation distribution factor*
$V_f + V_m = 1$
x=c=composite, f=fibre, m=matrix

Equation 4: Rule of Mixtures (Grove, 2018). Tensile Strength

Kelly-Tyson model

Equation 5 shows the Kelly-Tyson model for theoretical upper bound for tensile strength for unidirectional composites.

$$\sigma_c = \sigma_f V_f + \sigma_{m*} V_m$$

σ_c=*Predicted ultimate tensile strength (Pa)*
σ_f=*Ultimate tensile strength of fibre (Pa)*
V_f=*Fibre volume fraction*
σ_{m*}=*Tensile stress in matrix at failure strain of the fibre (Pa)*
V_m=*Matrix volume fraction*

Equation 5: Kelly-Tyson Model (Kelly and Tyson, 1965).

Assumed failure strain

Equation 6 shows assumed failure stress of 0.25% the to predict the lower bound flexural strength, where the composite tensile modulus used comes from Equation 4 This equation is a rearrangement of the Young's Modulus definition E=σ/ε.

$$\sigma_c = E_c \varepsilon'_c$$

σ_c = *Composite Tensile Strength (Pa)*
E_c = *Composite Tensile Modulus (Pa)*
ε'_c = *Assumed Failure Strain*

Equation 6: Composite strength using assumed strain (Grove, 2018).

Statistical Analysis

Experimental datasets were analysed, using version 25 of Statistical Package for the Social Sciences (SPSS) Statistics software. SPSS is a very versatile and advanced software package facilitating complex analysis. Groups were assumed to be parametric and statistical differences were evaluated using a one-way analysis of variance (ANOVA) with Tukey post hoc test. A 95% confidence limit is used to evaluate significant statistical difference ($p < 0.05$). Letters (e.g. A,B) will be used to denote statistical subsets within groups. Experimental results are reported with standard deviation (SD), coefficient of variation (COV) and Number of Valid Observations (NOVO) values.

Results

Specimens

Raised Sections

An unintended consequence of using the pegs was the bridging of the vacuum bag over the pegs. Figure 15 shows this affect as well as the raised sections formed. However, this does mimic the similar features in knots, shown in figure 16.

Figure 15: Left: bridging of vacuum bag, right: resulting raised sections around holes.

Figure 16: Plank section showing raised feature in in knot.

Resin Damage Defects

The drilling caused localised delamination whereas some of the raised sections had fractured resin caused by demoulding, these affects can be seen in figure 17.

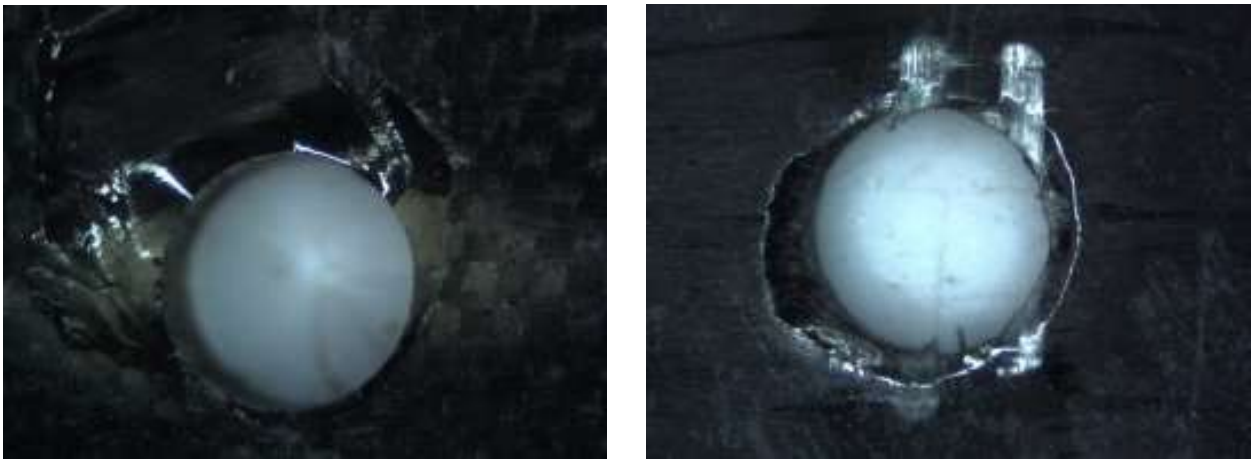

Figure 17: Detail of fractured resin around holes, left moulded hole and right drilled hole.

Specimen Details

Due to the stitching in the reinforcement the specimens differed slightly. Appendix 10.11 shows additional details of cross stitch position and tow relative to the hole as well as additional information about the failure including the largest ply remnants. Figures 18 and 19 illustrate these differences.

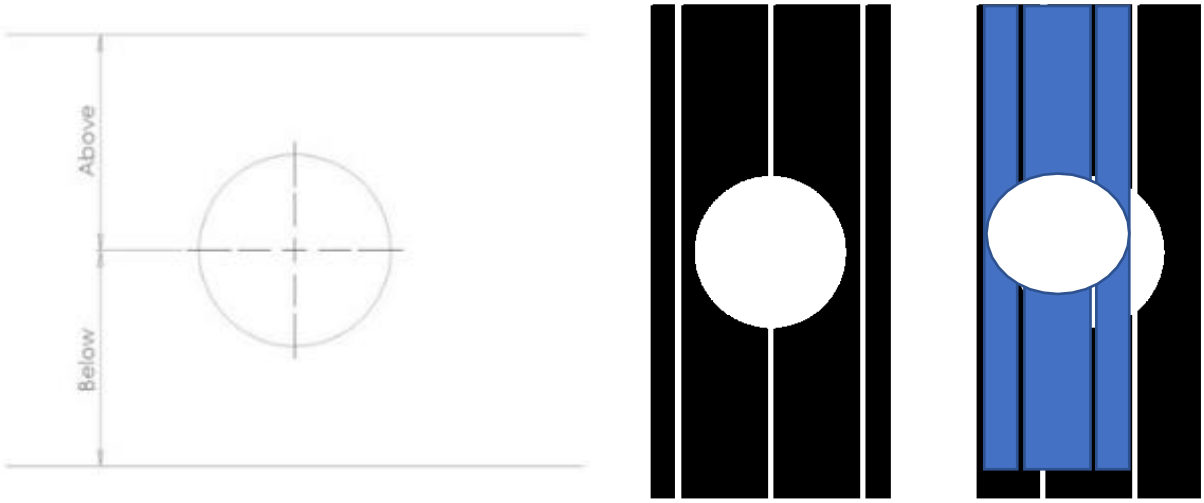

Figure 18: Illustration of stitch relative to centre of the hole. **Figure 19**: Hole relative to tow, left in between tows, right, though a tow.

Panel Dimensions

Appendix 10.9 gives details of specimen thickness and width. Figure 20 shows that the holes 4mm in diameter for plate types.

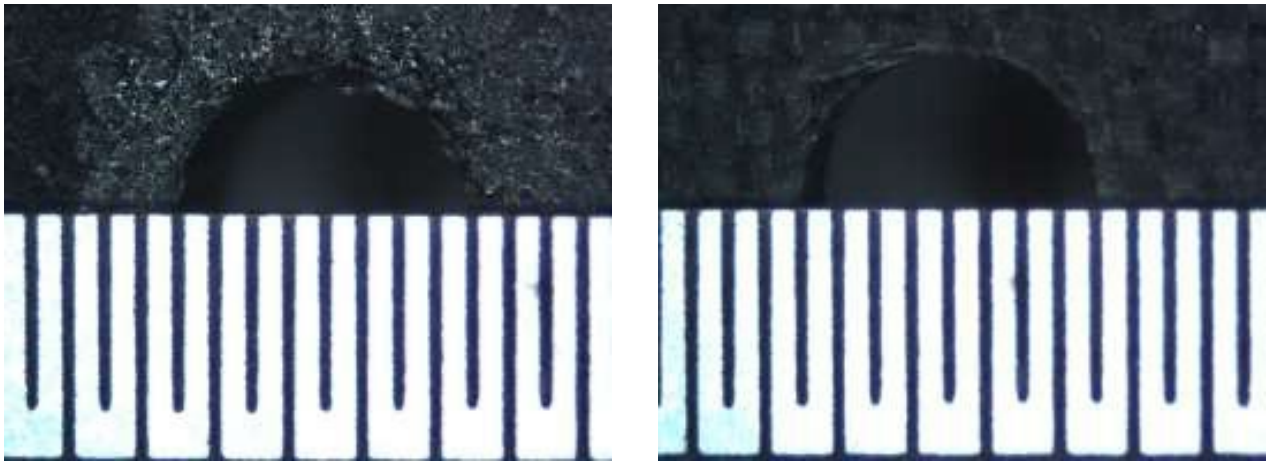

Figure 20: Holes with 0.5mm scale rule, left moulded and right drilled.

Surface Finish

Surface finish of plate A was mirror finished, whereas the moulded specimens resulted in a matt finish see Figure 21. Additionally, the mould did stick to the plate despite the addition of release agent. The resultant finishes affected the ability to see the tows and stitches see Figure 22.

Figure 21: Left: resin seep around the mould tool, right: mirror like surface of plate A.

Figure 22: Left: drilled plate, tows and stitches can clearly be seen, right: moulded specimen, tows and stitches are not as clear.

Failure modes

The tensile specimens were considered valid if they failed in the following ways which are illustrated in figures 23 and 24:

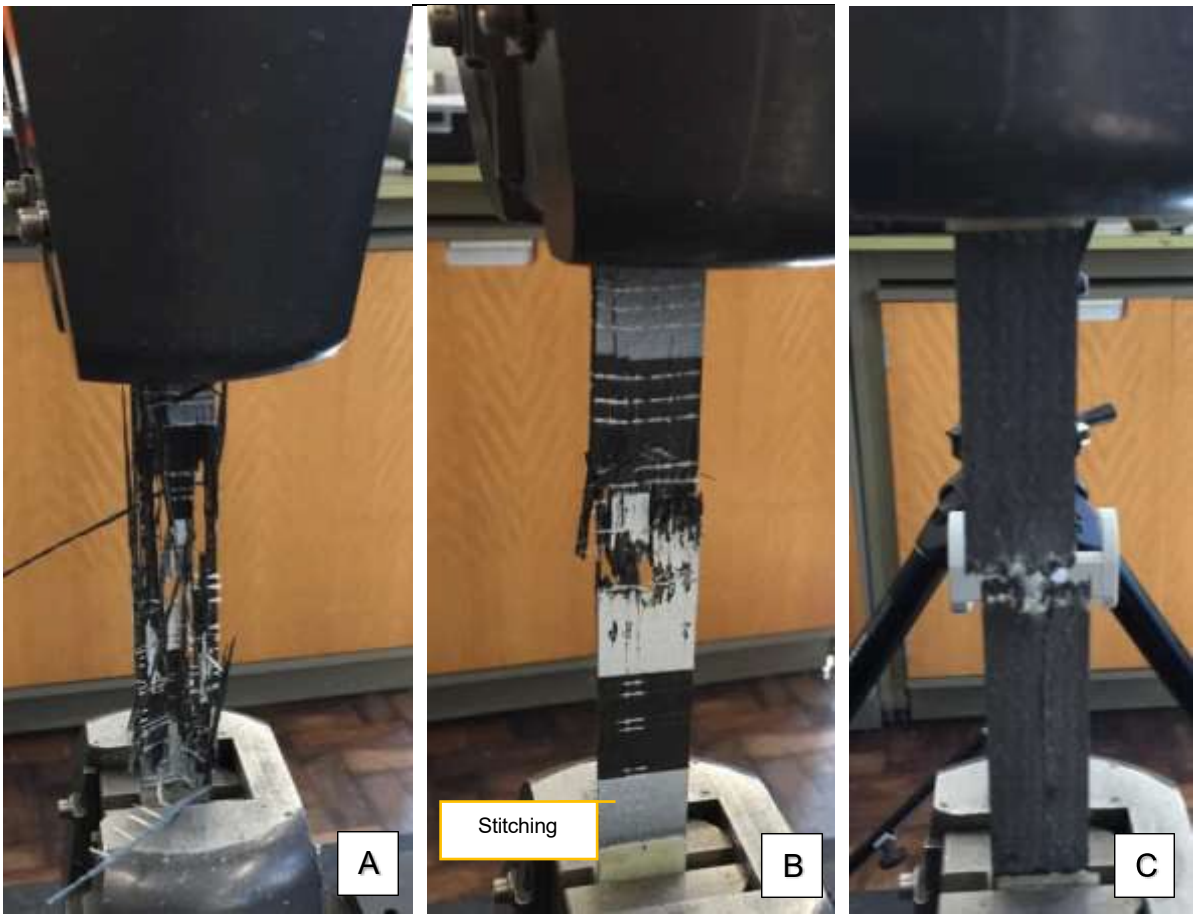

Figure 23: Specimen failure modes.

A. Fibre pull out along whole gauge length
B. Fibre pull out along whole gauge length but in two sections with substantial ply laminates
C. Failure laterally across the centre of the holes
D. Fracture from the either side of the hole.

The specimens from plate A (control and drilled) failed by modes A and B whilst plate B (moulded) failed in type C. Specimens which did not fail in these ways were due to slipping, these specimens were neglected from the experimental results analysis. Additionally, the UD nature of the specimens leads to this failure along the axis of tow. Each tow acted independently to each other which is shown in figure 23B, where the cross stitch has experienced stress whitening in line with a single tow which acted as a weak segment. Specimens O and R which were DIC specimens failed in another way shown in figure 24. These were the only examples to fail like this.

Figure 24: Fourth failure mode.

Fibre Volume Fraction

The various values for the volume fraction can be seen in Table 4. These three values will be used separately in the predictions of tensile strength and modulus.

Table 4: Volume fraction results, showing variation, COV.

Vf Method	Fibre Volume Fraction (%)
Thickness	51.55±0.75 (1.4%)
Burn-off	57.87±7.38 (12.7%)
Density	64.83±3.21 (4.9%)

Tensile Modulus

Table 5 presents the experimental tensile modulus results for all specimen types. The RoM tensile modulus prediction was calculated using the three volume fraction results, these can be seen in Table 6.

Table 5: Experimental tensile modulus values, showing variation, COV and NOVO.

Plate	Tensile Modulus (GPa)
Control	37.03±3.51 (9.5%) 6/6
Drilled	36.88±4.32 (11.7%) 10/10
Moulded	38.89±2.06 (5.3%) 10/10

Table 6: Rule of mixtures tensile modulus predictions using mean Vf.

Vf Method	Tensile Modulus (GPa)
Thickness	119.93
Burn-off	153.07
Density	150.10

Tensile Strength

Table 7 presents the experimental tensile strength results for all specimen types. The upper and lower bound tensile strength predictions can be seen in Table 8.

Table 7: Experimental tensile strength values, showing variation, COV and NOVO.

Plate	Tensile Strength (GPa)
Control	1.20±0.28 (23.1%) 5/6
Drilled	1.11±0.16 (14.1%) 9/10
Moulded	0.92±0.09 (9.9%) 10/10

Table 8: Kelly-Tyson and assumed failure strain tensile strength predictions using mean Vf.

	Tensile Strength (GPa)	
Vf Method	**Kelly-Tyson**	**Assumed failure strain**
Thickness	2.54	0.300
Burn-off	3.25	0.383
Density	3.18	0.375

Digital Image Correlation

The results are shown in figures 25 and 26 which illustrate the difference in how the crack propagated for each specimen type. Full results can be seen in appendix 0. It can clearly be seen that speckle pattern was more successful on plate A because of its polished mirror surface.

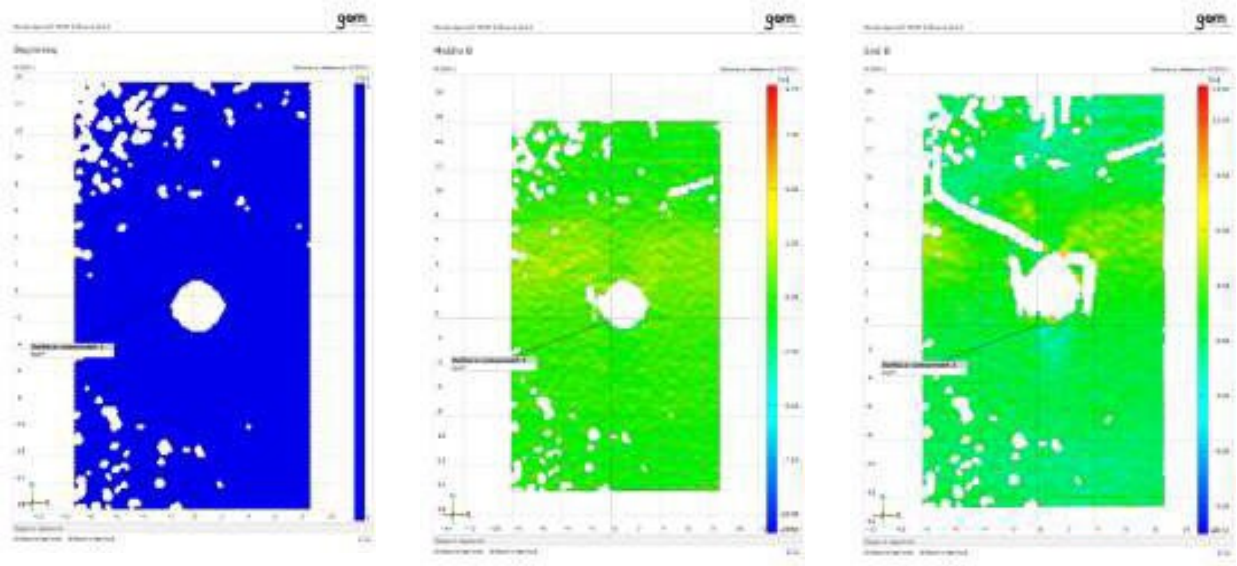

Figure 25: Specimen B, Indicative crack propagation of moulded specimen, beginning, start of crack propagation and end of test.

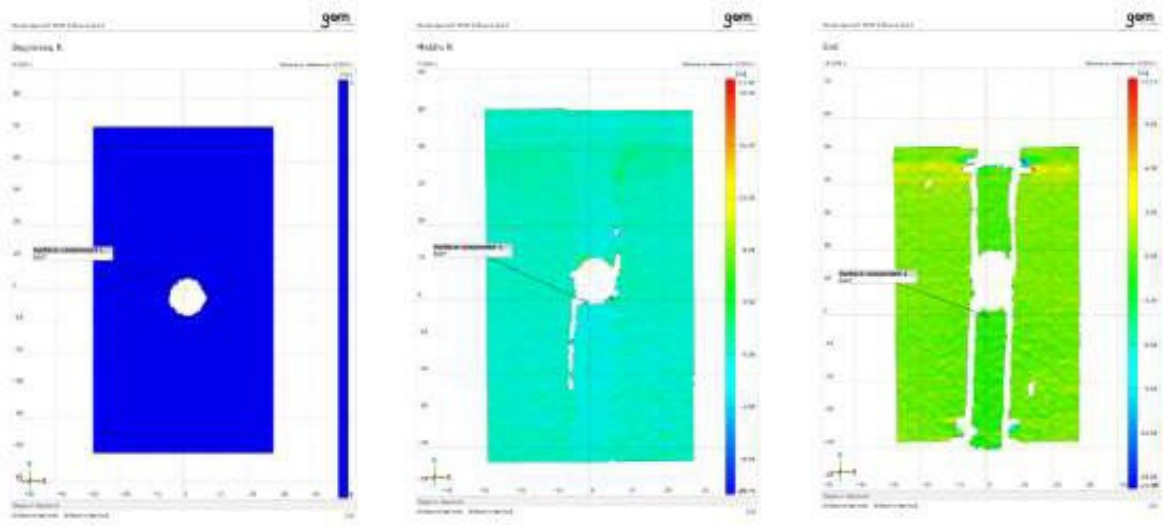

Figure 26: Specimen R, Indicative crack propagation of drilled specimen, beginning, start of crack propagation and end of test.

Discussion

Manufacture

The RIFT method produced plates that met the intended thickness of 2mm and the 4mm holes were very accurate. Whilst a true comparison between the three specimen types was planned, the reality of manufacturing lead to an additional variable. The drilled and control specimens came from the same plate whilst the moulded specimens were made separately due to circumstances beyond the author's control. The differences include, the resin used came from different batches, lab conditions varied on each day, the consumables may have differed, and the vacuum achieved was different for both. However, the most obvious difference was the use of a mould which caused a

different surface finish on the mould side and the raised section around the moulded holes. Furthermore, both plates were waterjet cut on different occasions and the moulded specimens were still attached to the mould, also the holes were premade, and a slight registration error led to the holes being 1mm off centre. Therefore, the experimental results may have been impacted by these issues.

Although, this mould method may give lower tensile strength, from an environmental and scientific point of view it is beneficial; as the pegs are reusable, will save on machining time and cost of replacing carbide drill bits. It was quicker to produce the moulded holes in the University context and it is more reproducible, should further study be required.

Fibre Volume Fraction

Figure 27, shows the calculated (Thickness) and experimental (Burn-off and Density) values of the fibre volume fraction. All of the values fit between the indicative 50%-70% for UD composites (Grove, 2018) and show no statistically significant difference. The thickness method gives the lowest value, followed by resin burn off and then the density method. All the mean values fall between the error bars of the burn off method suggesting agreement. However, both experimental methods are only based on 2 results one from plate A and one from plate B which reduces the reliability of the results.

The limitation of the thickness method is that it does not take account of the topography if the surface finish. It only measures across the peaks, which arise from the surface finish, caused by the peel ply and thus underestimates the Vf. However, it is based on the values of all specimens' thicknesses and has a lower COV.

Additionally, these methods rely on the assumed fibre and resin densities which may not be accurate, or representative of the actual materials used. Figure 28, shows the graph used for the density method, if the assumed values were different the blue line would have a different gradient.

The carbon fibre used was not suitable for resin burn off as 79% of the control fibre mass was lost and an unknown proportion of this was surface treatment so some of the carbon burnt off. Therefore, the correction made for this might not be entirely accurate as it is only based on one control sample.

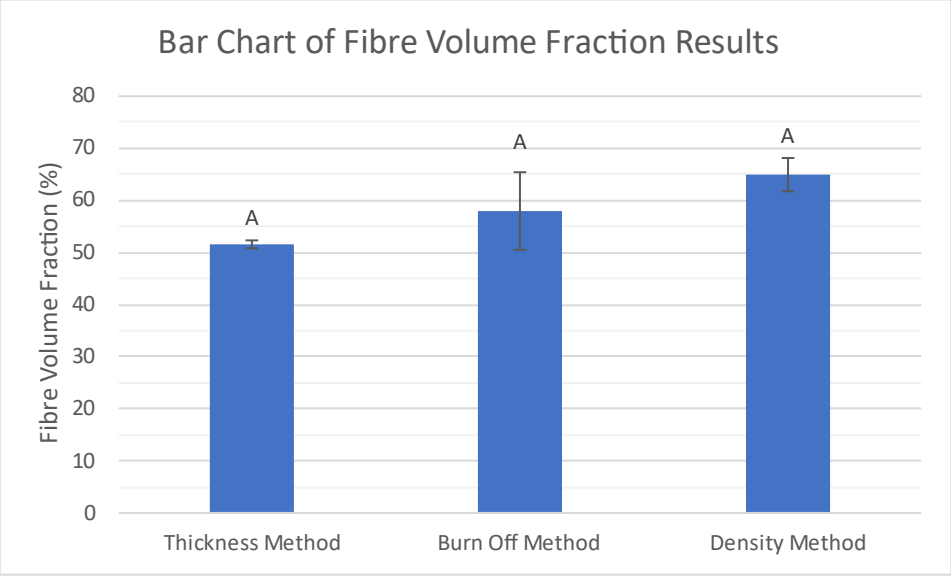

Figure 27: Bar chart of fibre volume fraction results.

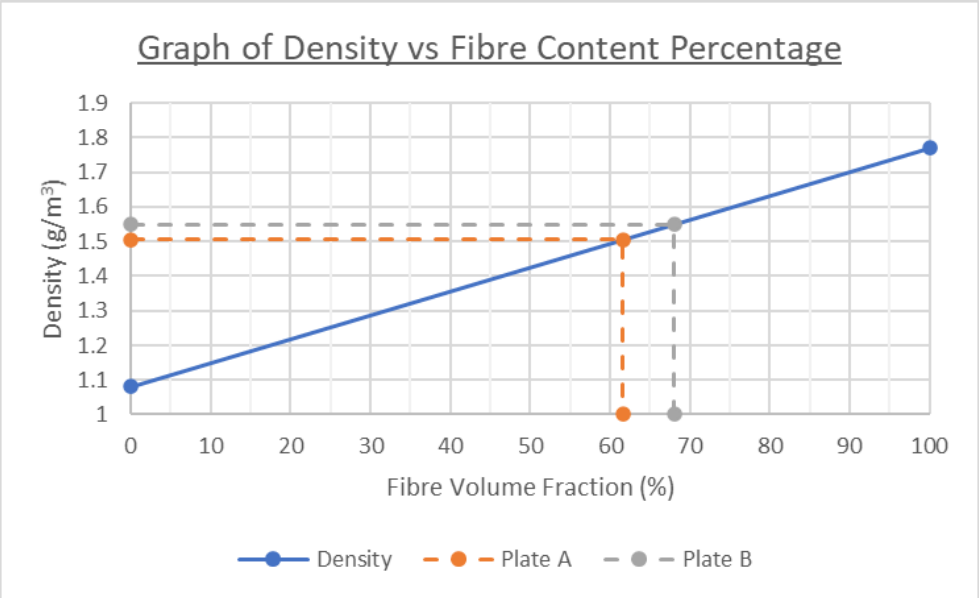

Figure 28: Graph of density vs fibre content percentage.

Tensile Results

Tensile Modulus

All the experimental modulus results in figure 29 show agreement as the values fit in a statistically identical region (37.6±0.9GPa). The moulded plates show a slight 5.0% increase when compared to the control specimen and are more consistent this might be since they were manufactured under slightly different conditions. However, this insignificant difference shows that the manufacturing gives consistent material properties.

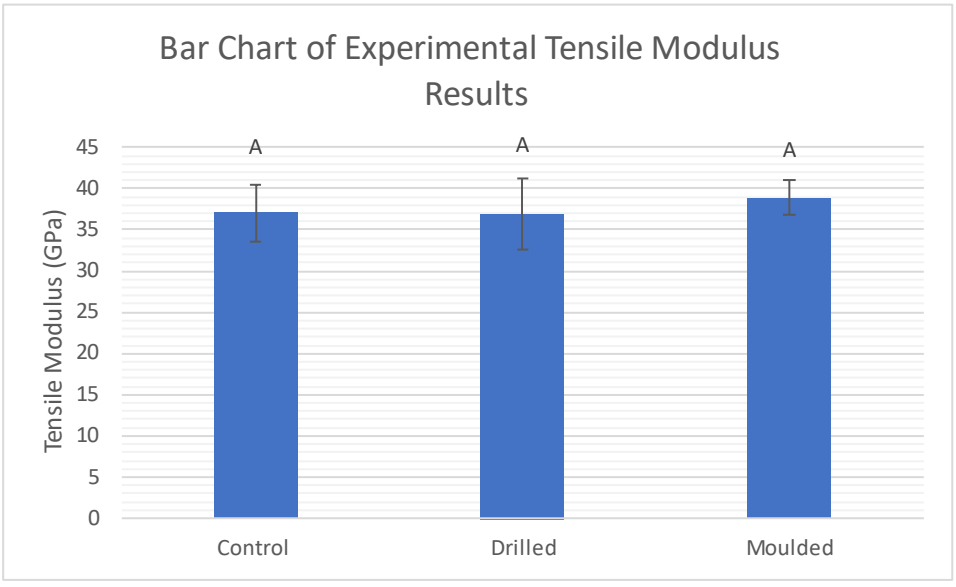

Figure 29: Bar chart of experimental tensile modulus results.

Figure 30, shows the experimental control value compared to the RoM prediction using all Vf values. This shows that the achieved experimental strength reaches between 24%- 31% of the prediction.

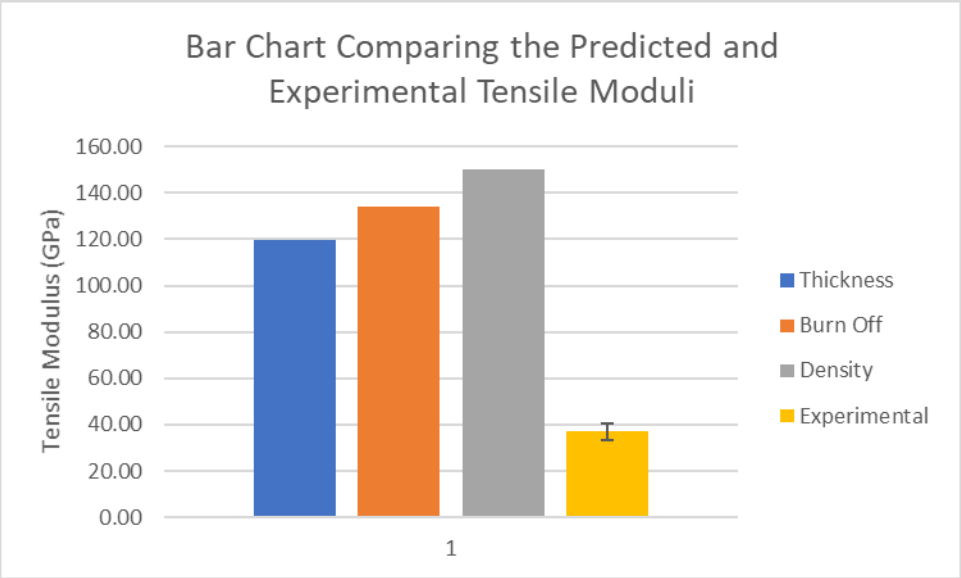

Figure 30: Bar chart comparing the predicted and experimental tensile moduli.

Tensile Strength

The experimental strength results in figure 31, indicate that the moulded specimens are significantly weaker (76.4%) whilst the drilled (92.5%) show no statistically significant difference when compared to the control plate. The moulded holes did not meet expectations, but did not have a valid control, as the control was from plate A, so might not be fully comparable, however as shown in figure 29 the material properties were the same. Additionally, the raised sections and the different failure modes imply variance due to surface topology. Furthermore, by redirecting the fibres around the hole a resin rich volume (RRV) was formed, unintentionally increasing the hole size, see figure 32. The larger hole causes a stress concentration which is exacerbated by the RRV. The RRV negatively affects the mechanical properties of composites, because they cause stress concentrations and are linked to crack initiation and propagation (Mahmood et al., 2022).

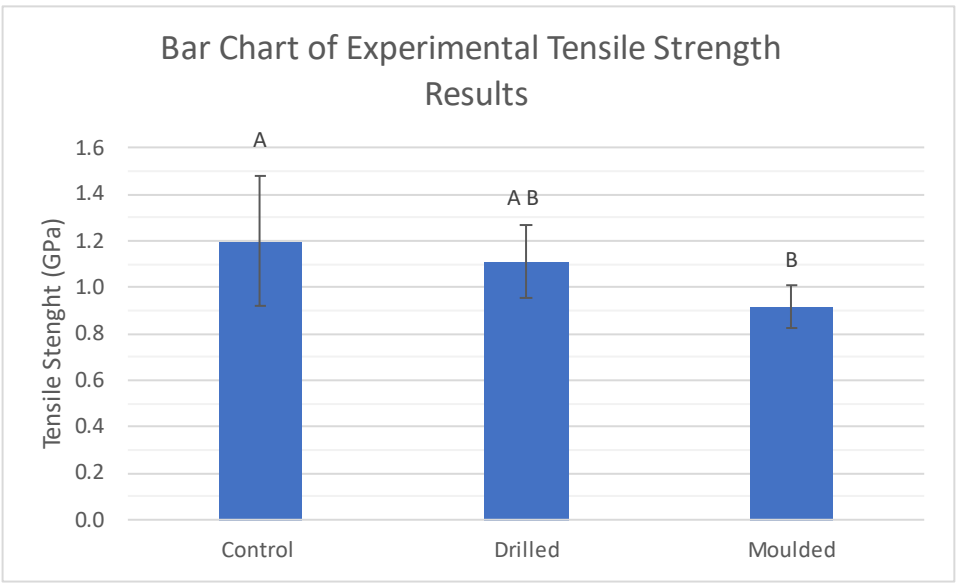

Figure 31: Bar chart of experimental tensile strength results. **Figure 32:** Resin rich volume formed around moulded hole.

Figure 33, shows the experimental control value compared to both Kelly-Tyson and assumed strain predictions using all Vf values. This shows the experimental results are sensible as they fall between the upper and lower bound predictions. Indicating that the achieved experimental strength reaches between 37%-47% of the Kelly-Tyson prediction.

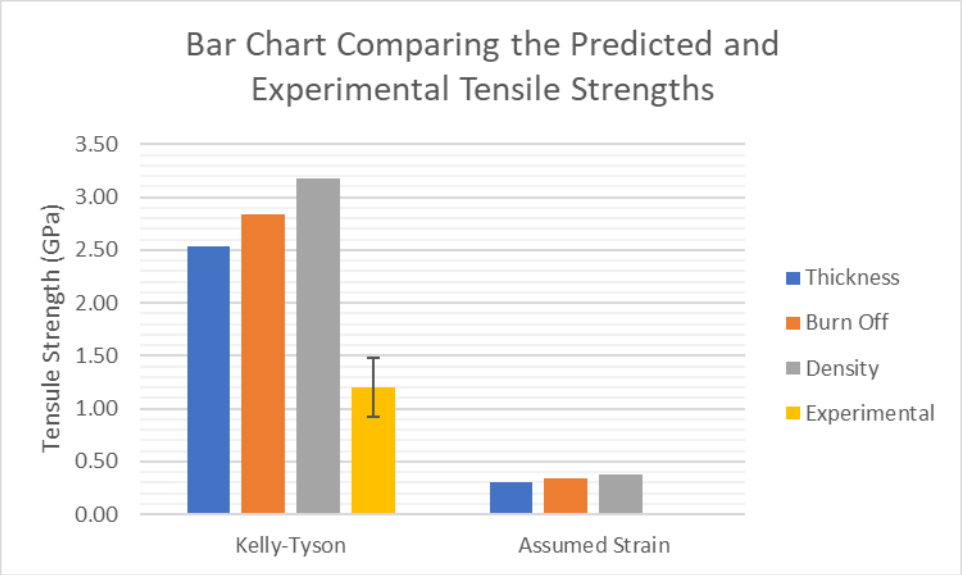

Figure 33: Bar chart comparing the predicted and experimental tensile strengths.

General

The strength of the plates is 14.7% closer to predictions than the modulus. However, all the values are lower than the predictions which could be due to defects in the matrix, like voids or slight misalignment in tensile machine or within the composite itself. Also, each layer is not identical in terms of stitch and tow positions. Additionally, the fibre properties used in the prediction calculations were for virgin fibre although over 19 years the surface treatment may have deteriorated or have been removed. Furthermore, it has been handled and manipulated by students and the fibre values do not account for diminished properties due to the textile process. Also, the resin properties may not have been reached due to aging or improper storage.

Additionally, results may not be fully accurate as the tensile machine was out of calibration. And the assumptions used in the predictions may not be valid. The location of the stitching and tows in the top layer did not appear to affect the results.

The failure of the moulded specimens was not as catastrophic as plate A which would be beneficial for damage monitoring in the life cycle of a product manufactured in this way. Additionally, the failed moulded specimens were safer as they did not create sharp spikes or explode. Furthermore, there is no wasted material or risk of delamination and dust when installing components.

DIC

Unfortunately, due to the brittle nature of the specimens and the poor resolution of the speckle surface, meaningful strain data could not be gathered. Because of the

brittleness of the sample the localised movement of the speckles was too small to be registered. However, from the images it is possible to deduce and visualise the crack propagation due to the lack of data where the white spots appear.

Therefore, interpreting the results can give a qualitative comparison of the different failure modes of the drilled and moulded plates. The drilled plates fail in large scale fibre pull out starting at the holes which is similar to the control, whilst the moulded plates fail across the specimen starting at the hole. This shows completely different failure modes, possibly due to differences in resin curing as well as the raised section which changes the CSA.

Recommendations

Property Prediction

- Conduct single fibre tensile tests on the actual fabric used so that the predictions will be more relevant. Additionally, this will quantify the amount that textile processing and handling in the workshop diminishes the properties when compared to virgin fibre.
- Pre heat resin and use from same batch to minimise property variance.

Raised Section

- Alter the mould to use an upper flat plate to stop the bridging of the draping infusion film.
- Different material for pins or manufactured elsewhere so that it could be made shorter, so the bridging doesn't occur.

Ease of Testing

- Make thinner tabs so that the specimens do not get jammed in the tensile vice every time.

Creating a Fairer Test

- Either make control from each plate or make all samples types out of the same plate.
- Make a mould tool with better registration and possibly out of metal so it can be polished and the difference in surface finish can be negated.
- Alternate control specimen with moulded to reduce any regional affect within the plate.
- Increase number of test samples.

Improving Value of Findings

- Use alternative material and weave types to better reflect the use context, as composite industry does not purely use carbon UD.
- Use different sized holes to see if scale affects the results.
- Make FEA model with a closer representation of the fibre orientation around

holes so results can be properly validated and in future this model might be able to predict different hole ratios and materials and layup.

- Properly record the location of the stitch relative to the hole during manufacture to investigate its effect on results.
- Improve the quality of the DIC speckle pattern through trials and possibly use stereo for 3D data if the raised sections occur again.

Conclusions

The aim of this report was to compare the mechanical performance of two methods of creating holes in composites manufactured using the RIFT method. The research led to the use of tree knot holes as the model for producing holes with continuous fibres due to their fibrous construction. A mould was designed and implemented to facilitate the realisation of this inspiration in a physical test sample. Based on the methodology, assumptions and flaws previously discussed the following conclusions can be made:

1. The experimental tensile strength results are 14.7% closer to predictions than the modulus predictions when using the same material properties.
2. According to the study the moulded holes strength performed 16.2% weaker than the drilled plates when compared to the control specimens.
3. The tensile modulus results of 37.6±0.9 GPa indicates a minor variation but essentially agree with each other.
4. Plates A and B had different failure modes; the moulded specimens failed more gradually.
5. Test results show that the advantages of premade holes using this method could be exploited in real world situations.
6. The location of tow and stitching in the top layer did not appear to affect the results.

Acknowledgements

I would like to express my gratitude to:

- Prof John Summerscales my supervisor for sharing his knowledge on composite materials and helping and guiding me in manufacturing the composite panels and project generally.
- Neil Fewings, Dave Patterson (Brunel W6) and Hannah Carter (Smeaton workshop) technicians who aided in producing the mould tool and drilled specimens.
- Dr Jeremy Clark and Katie Shore (Smeaton 001) technicians, for their assistance with carrying out the mechanical testing and optical analysis of the specimens.
- Dr Xinyu Wang for his assistance and guidance with the digital image correlation.
- Kate Russell, for acquiring the necessary standards and advice.

Nomenclature

Symbol	Property	Unit
a	Composite Weight in Air	g
ACP	Ansys Composite PrepPost	-
Af	Areal Weight	g/cm^2
ANOVA	Analysis of Variance	-
b	Composite Weight in Water	g
COV	Coefficient of Variation	%
CSA	Cross-sectional Area	m^2
CRAG	Composite Research Advisory Group	-
d	Diameter	m
DIC	Digital Image Correlation	-
Ec	Composite Tensile Modulus	Pa
Ef	Fibre Tensile Modulus	Pa
Em	Matrix Tensile Modulus	Pa
FEA	Finite Element Analysis	-
L	Length	m
Mf	Mass of Fibres	g
Mc	Mass of Composite	g
n	Number of Layers	-
NOVO	Number of Valid Observations	-
RIFT	Resin Infusion Under Flexible Tooling	-
RoM	Rule of Mixtures	-
RRV	Resin Rich Volume	
SD	Standard Deviation	-
SPSS	Statistical Package for the Social Sciences	-
t	Thickness	m
UD	Unidirectional	-
W	Width	m
Vf	Fibre Volume Fraction	%
Vm	Matrix Volume Fraction	%
ε'c	Assumed Failure Strain in the Composite	-
ηd	Fibre Diameter Distribution Factor	-
ηl	Fibre Length Distribution Factor	-
ηo	Fibre Orientation Distribution Factor	-
κ	Fibre Area Correction Factor	-
ρc	Composite Density	kg/m^3
ρf	Fibre Density	kg/m^3
ρw	Water Density	kg/m^3
σc	Composite Tensile Strength	Pa
σf	Fibre Tensile Strength	Pa
σm	Matrix Tensile Strength	Pa
σ^*m	Tensile Stress in the Matrix at Failure Strain of the Fibre	Pa

Reference List

Abd, H. M., Magdy, N. and Sameh, H. (2018). *Bio-mimicry as a tool for minimizing energy consumption and improvement of thermal comfort: The case of office buildings*. In: 2018. London.

Adamu, Z. and Price, A. (2015). Natural Ventilation with Heat Recovery: A Biomimetic Concept. *Buildings*, 5 (2), pp.405–423. [Online]. Available at: doi:10.3390/buildings5020405.

Alderson, E. (2019). *Why Are so Many Objects in the Universe Round?* Predict. [Online]. Available at: https://medium.com/predict/why-are-so-many-objects-in-the-universe-round-7eca8c3305fc [Accessed 25 March 2022].

Åström, B. T. (2017). *Manufacturing of Polymer Composites*. 1st ed. Routledge. [Online]. Available at: doi:10.1201/9780203748169 [Accessed 22 November 2021].

Barbero, E. J. (1999). *Introduction to composite materials design*. Philadelphia: Taylor and Francis.

Bar-Cohen, Y. (Ed). (2006). *Biomimetics: biologically inspired technologies*. Boca Raton, FL: CRC/Taylor & Francis.

Boaretto, J. et al. (2021). Biomimetics and Composite Materials toward Efficient Mobility: A Review. *Journal of Composites Science*, 5 (1). [Online]. Available at: doi: https://doi.org/10.3390/jcs5010022

Burns, L. A. et al. (2012). Bio-inspired design of aerospace composite joints for improved damage tolerance. *Composite Structures*, 94 (3), pp.995–1004. [Online]. Available at: doi: https://doi.org/10.1016/j.compstruct.2011.11.005

Cho, H. K. and Rowlands, R. E. (2009). Optimizing Fiber Direction in Perforated Orthotropic Media to Reduce Stress Concentration. *Journal of Composite Materials*, 43 (10), pp.1177–1198. [Online]. Available at: doi: https://doi.org/10.1177/0021998308103608

Clyne, T. W. and Hull, D. (2019). *An introduction to composite materials*. Third. Cornwall: Cambridge University Press.

Cripps, D. (2019). *Fatigue Resistance*. Composites World. [Online]. Available at: https://netcomposites.com/guide/resin-systems/fatigue-resistance/ [Accessed 13 November 2021].

Dantec Dynamics. (2022). *Speckle Pattern Application*. Dantec Dynamics. [Online]. Available at: https://www.dantecdynamics.com/components/speckle-pattern-application/?sourceid=1038 [Accessed 9 April 2022].

Dickinson, M. H. (1999). Bionics: Biological insight into mechanical design. *Proceedings of the National Academy of Sciences*, 96 (25), pp.14208–14209. [Online]. Available at: doi:10.1073/pnas.96.25.14208.

Duran, F. (2015). *Radiolaria, Plankton Fossil*. Pixabay. [Online]. Available at: https://pixabay.com/photos/radiolaria-plankton-fossil-936194/ [Accessed 3 July 2023].

Easy Composites. (n.d.). *IN2 EPOXY INFUSION RESIN - Technical Datasheet*. Easy Composites. [Online]. Available at: https://media.easycomposites.co.uk/datasheets/EC-TDS-IN2-Infusion-Resin.pdf [Accessed 12 March 2022].

Fu, S.-Y. et al. (2000). Tensile properties of short-glass-fiber- and short-carbon-fiber-reinforced polypropylene composites. *Composites Part A: Applied Science and Manufacturing*, 31 (10), pp.1117–1125. [Online]. Available at: doi: https://doi.org/10.1016/S1359-835X(00)00068-3

Galińska, A. (2020). Mechanical Joining of Fibre Reinforced Polymer Composites to Metals—A Review. Part I: Bolted Joining. *Polymers*, 12 (10), p.2252. [Online]. Available at: doi:10.3390/polym12102252.

Götz, K. and Mattheck, C. (2001). Trees as a model for technical fibre composites. In: *Proceedings of the International Conference on Computer Aided Optimum Design of Structures*. 7. 2001. OPTI. pp.391–400.

Grove, S. (2018). *Composite materials and structures for engineering students*. Great Britain: Kindle Direct Publishing.

Guo, S. J. (2007). Stress concentration and buckling behaviour of shear loaded composite panels with reinforced cutouts. *Composite Structures*, 80 (1), pp.1–9. [Online]. Available at: doi:10.1016/j.compstruct.2006.02.034.

Hu, F. Z., Soutis, C. and Edge, E. C. (1997). Interlaminar stresses in composite laminates with a circular hole. *Composite Structures*, 37 (2), pp.223–232.

Jungnikl, K. et al. (2009). The role of material properties for the mechanical adaptation at branch junctions. *Trees*, 23 (3), pp.605–610. [Online]. Available at: doi:10.1007/s00468-008-0305-9.

Kelly, A. and Tyson, W. R. (1965). Tensile properties of fibre-reinforced metals: Copper/tungsten and copper/molybdenum. *Journal of the Mechanics and Physics of Solids*, 13 (6), pp.329–350. [Online]. Available at: doi:10.1016/0022-5096(65)90035- 9.

Kidd, D. (2019). *amber lighted ceiling*. Unsplash. [Online]. Available at: https://unsplash.com/photos/_w0ETDhqEBc [Accessed 3 July 2023].

Kumar, S. A., Rajesh, R. and Pugazhendhi, S. (2020). A review of stress concentration studies on fibre composite panels with holes/cutouts. *Proceedings of the Institution of Mechanical Engineers, Part L: Journal of Materials: Design and Applications*, 234 (11), pp.1461–1472. [Online]. Available at: doi:10.1177/1464420720944571.

Lal, A., Sutaria, B. M. and Kumar, R. (2020). Bending analysis of a sandwich plate with elliptical/circular cutout. *IOP Conference Series: Materials Science and Engineering*, 1004, p.012019. [Online]. Available at: doi:10.1088/1757- 899X/1004/1/012019.

Lin, M. J., Tsai, K. H. and Hwan, C. L. (2020). Strength Prediction for Composite Plates with an Inclined Elliptical Hole. *Mechanics of Composite Materials*, 56 (5), pp.619–628. [Online]. Available at: doi:10.1007/s11029-020-09908-z.

Mahmood, A. S., Summerscales, J. and James, M. N. (2022). Resin-Rich Volumes (RRV) and the Performance of Fibre-Reinforced Composites: A Review. *Journal of Composites Science*, 6 (2), p.53. [Online]. Available at: doi:10.3390/jcs6020053.

Malakhov, A. V. and Polilov, A. N. (2016). Design of composite structures reinforced curvilinear fibres using FEM. *Composites Part A: Applied Science and Manufacturing*, 87, pp.23–28. [Online]. Available at: doi:10.1016/j.compositesa.2016.04.005.

McGrane, R. A. (2001). *Vacuum Assisted Resin Transfer Molding of Foam Sandwich Composite Materials: Process Development and Model Verification*. Master of Science, Blacksburg, Virginia: Virginia Polytechnic Institute and State University.

Mendoza Jasso, A. J. et al. (2011). A parametric study of fiber volume fraction distribution on the failure initiation location in open hole off-axis tensile specimen. *Composites Science and Technology*, 71 (16), pp.1819–1825. [Online]. Available at: doi:10.1016/j.compscitech.2011.08.008.

Mohamed Makki, M. and Chokri, B. (2017). Experimental, analytical, and finite element study of stress concentration factors for composite materials. *Journal of Composite Materials*, 51 (11), pp.1583–1594. [Online]. Available at: doi:10.1177/0021998316659915.

O'Dogherty, L., Suzuki, N. and Goričan, Š. (2021). Radiolaria (Polycystinea). In: *Encyclopedia of Geology*. Elsevier. pp.420–434. [Online]. Available at: doi:10.1016/B978-0-08-102908-4.00143-0 [Accessed 25 November 2021].

Polilov, A. N. and Tatus, N. A. (2020). Biomimetic design of fibrous composite structures. In: *IOP Conference Series: Materials Science and Engineering*. 1129. 2020. Moscow Russia. [Online]. Available at: doi: https://doi.org/10.1088/1757-899X/1129/1/012022

Pu, X., Li, G. and Huang, H. (2016). Preparation, anti-biofouling and drag-reduction properties of a biomimetic shark skin surface. *Biology Open*, 5 (4), pp.389–396. [Online]. Available at: doi:10.1242/bio.016899.

RAE. (1988). Crag test methods for the measurement of the engineering properties of fibre reinforced plastics. curtis, p. t. (ed). Royal Aerospace Establishment.

Round, F. E., Crawford, R. M. and Mann, D. G. (1990). *The Diatoms: biology & morphology of the genera*. Cambridge [England] ; New York: Cambridge University Press.

Slayton, R. and Spinardi, G. (2016). Radical innovation in scaling up: Boeing's Dreamliner and the challenge of socio-technical transitions. *Technovation*, 47, pp.47–58. [Online]. Available at: doi: https://doi.org/10.1016/j.technovation.2015.08.004

Sloan, J. (2012). *A400M wing assembly: Challenge of integrating composites*. Composites World. [Online]. Available at: https://www.compositesworld.com/articles/a400m-wing-assembly-challenge-of-integrating-composites [Accessed 22 November 2021].

Sofianto, I. A. et al. (2019). Effect of knots and holes on the modulus of elasticity prediction and mapping of sugi (Cryptomeria japonica) veneer using near-infrared hyperspectral imaging (NIR-HSI). *Holzforschung*, 73 (3). [Online]. Available at: doi: https://www.degruyter.com/document/doi/10.1515/hf-2018-0060/html

TEKU. (n.d). *PTFE - fluoroplastic - Properties and characterisic data*. TEKU GmbH Fluorkunststoffe.

Tenchev, R. T., Nygard, M. K. and Echtermeyer, A. (1995). Design procedure for reducing the stress concentration around circular holes in laminated composites. *Composites*, 26 (12), pp.815–828. [Online]. Available at: doi:10.1016/0010-4361(95)90875-Z.

Tsoumis, G. T. (1991). *Science and technology of wood: structure, properties, utilization*. New York: Van Nostrand Reinhold.

Vasiliev, V. V., Barynin, V. A. and Razin, A. F. (2012). Anisogrid composite lattice structures – Development and aerospace applications. *Composite Structures*, 94 (3), pp.1117–1127. [Online]. Available at: doi:10.1016/j.compstruct.2011.10.023.

Vincent, J. F. V. (2016). Biomimetics in architectural design. *Intelligent Buildings International*, 8 (2), pp.138–149. [Online]. Available at: doi:10.1080/17508975.2014.911716.

Warren, A. S. (2004). Developments and Challenges for Aluminum – A Boeing Perspective. *MATERIALS FORUM*, 28.

Watsar, S. D. and Bharule, A. (2015). Stress Analysis of Finite Plate with Special Shaped Cutout. *International Journal of Scientific Engineering and Research*

(IJSER), 3, pp.145–150.

Withey, P. A. (1997). Fatigue failure of the de Havilland comet I. *Engineering Failure Analysis*, 4 (2), pp.147–154. [Online]. Available at: doi:10.1016/S1350- 6307(97)00005-8.

Worrall, C., Kellar, E. and Vacogne, C. (2020). *JOINING OF FIBRE-REINFORCED POLYMER COMPOSITES: A Good Practice Guide*. Composites UK.

Yang, C.-L., Sheu, S.-H. and Yu, K.-T. (2008). Optimal machining parameters in the cutting process of glass fibre using the reliability analysis based on the Taguchi method. *Proceedings of the Institution of Mechanical Engineers, Part B: Journal of Engineering Manufacture*, 222 (9), pp.1075–1082. [Online]. Available at: doi:10.1243/09544054JEM1134.

Yeh, H. Y. and Le, M. D. (1991). Stresses of Composite Laminates Containing Holes and Cracks. In: Teoh, S. H. and Lee, K. H. (Eds). *Fracture of Engineering Materials and Structures*. Dordrecht: Springer. pp.170–175. [Online]. Available at: https://doi.org/10.1007/978-94-011-3650-1_23.

Yin, S. et al. (2020). Tough Nature-Inspired Helicoidal Composites with Printing-Induced Voids. *Cell Reports Physical Science*, 1 (7), p.100109. [Online]. Available at: doi:10.1016/j.xcrp.2020.100109.

Zhang, J. et al. (2021). Effect of Hole Arrangement on Failure Mechanism of Multiple-Hole Fiber Metal Laminate under On-Axis and Off-Axis Loading. *Materials*, 14 (19), p.5771. [Online]. Available at: doi:10.3390/ma14195771.

Appendices are provided separately as supplementary files (see additional downloads for this article).